Nonlinear Phenomena in Complex Systems, vol. **11**, no. 2 (2008), pp. 171 - 176

Studying the Global Dynamics of Conservative Dynamical Systems Using the SALI Chaos Detection Method

T. Manos*
Observatoire Astronomique de Marseille-Provence (OAMP), 2 Place Le Verrier, F–13248, Marseille, FRANCE

Ch. Skokos
Astronomie et Systèmes Dynamiques, Institut de Mécanique Céleste et de Calcul des Ephémérides (IMCCE), Observatoire de Paris, 77 avenue Denfert-Rochereau, F–75014, Paris, FRANCE

E. Athanassoula† and T. Bountis‡
† *Observatoire Astronomique de Marseille-Provence (OAMP), 2 Place Le Verrier, F–13248, Marseille, FRANCE*
‡ *Center for Research and Applications of Nonlinear Systems (CRANS), Department of Mathematics, University of Patras, GR–26500, GREECE*
(Received 11 January, 2008)

We use the Smaller ALignment Index (SALI) method of chaos detection, to study the global dynamics of conservative dynamical systems described by differential or difference equations. In particular, we consider the well–known 2–dimensional standard map and autonomous Hamiltonian systems of 2 and 3 degrees of freedom describing the motion of a star in models of barred galaxies. The application of SALI helped us to compute rapidly and accurately the percentage of regular and chaotic motion for particular values of the parameters of these systems. We were also able to perform a computationally efficient determination of the dependence of these percentages on the variation of various parameters of the studied models.

PACS numbers: 92.87; 96.35.-j
Keywords: symplectic maps, hamiltonian systems, standard map, barred galactic potentials, chaotic motion, regular motion, SALI method

1. Introduction

The qualitative distinction between chaotic and regular motion in symplectic maps and in systems of differential equations is a fundamental problem of non–linear dynamics. This distinction is in general, a non trivial task and it becomes more difficult as the number of degrees of freedom increases. For this reason, over the years, several methods distinguishing regular from chaotic motion in conservative dynamical systems have been proposed and applied, with varying degrees of success.

One of the most efficient methods of chaos detection is the computation of the so-called **S**maller **AL**ignment **I**ndex (**SALI**) which was introduced in [1] and has already been applied successfully to several dynamical systems [1–18]. SALI has proved to be a fast and reliable method which can distinguish between regular and chaotic motion rapidly, reliably and accurately. These characteristics make the index a perfectly suited tool for the study of global dynamics of dynamical systems. For these reasons we use SALI to study the behavior of two distinct dynamical systems: the well–known 2–dimensional (2D) standard map [19] and Hamiltonian systems of 2 (2D) and 3 (3D) degrees of freedom, describing the motion of stars in models of barred galaxies. In the present paper, we present some preliminary results of our studies.

The paper is organized as follows: In Section 2 we recall the definition of SALI explaining also its behavior for regular and chaotic orbits. In Section 3 we use SALI for computing the fraction of chaotic orbits in the case of the standard map, while in Section 4 the results of an analogous study for Hamiltonian systems of barred galaxies are presented. Finally, in Section 5 we present our conclusions.

2. The Smaller Alignment Index (SALI)

Let us consider a l - dimensional phase space of a conservative dynamical system, which could be a $2M$-dimensional symplectic map or a Hamiltonian flow of N degrees of freedom, with $l = 2N$. We consider

*Also at Center for Research and Applications of Nonlinear Systems (CRANS), Department of Mathematics, University of Patras, GR–26500, GREECE

also an orbit in this space with initial condition $S(0) = (x_1(0), x_2(0), ..., x_l(0))$ and two deviation vectors $V_1(0) = (dx_{11}(0), dx_{12}(0), ..., dx_{1l}(0))$ and $V_2(0) = (dx_{21}(0), dx_{22}(0), ..., dx_{2l}(0))$, from the initial point $S(0)$.

For the computation of the SALI of a given orbit, one has to follow the time evolution of the orbit itself and also of two deviation vectors which initially point in two different directions. The evolution of an orbit of a map F is described by the discrete-time equations of the map:

$$S(n+1) = F(S(n)), \tag{1}$$

where $S(n) = (x_1(n), x_2(n), ..., x_l(n))$, represents the orbit's coordinates at the n-th iteration. The evolution of the deviation vectors $V_1(n), V_2(n)$, in this case, is given by the equations of the tangent map:

$$V(n+1) = DF(S(n)) \cdot V(n). \tag{2}$$

In the case of Hamiltonian flows the evolution of an orbit is given by the Hamilton's equation of motion:

$$\frac{dS(t)}{dt} = F(S(t)), \tag{3}$$

where F is a set of n-functions $(F_1, F_2, ..., F_n)$, while the corresponding evolution of the deviation vectors $V_1(t), V_2(t)$, is given by the variational equations:

$$\frac{dV(t)}{dt} = DF(S(t)) \cdot V(t) \ . \tag{4}$$

We note that in (2) and (4) DF denotes the Jacobian matrix of equations (1) and (3) respectively, evaluated at the points of the orbit under study.

At every time step (or iteration) the two deviation vectors $V_1(t)$ and $V_2(t)$ are normalized with norm equal to 1 and the SALI is then computed as:

$$SALI(t) = min\left\{ \left\| \frac{V_1(t)}{\|V_1(t)\|} + \frac{V_2(t)}{\|V_2(t)\|} \right\|, \left\| \frac{V_1(t)}{\|V_1(t)\|} - \frac{V_2(t)}{\|V_2(t)\|} \right\| \right\}, \tag{5}$$

where $\|\cdot\|$ denotes the usual Euclidean norm and t is the continuous or discrete time.

SALI has a completely different behavior for regular and chaotic orbits and this allows us to clearly distinguish between them. In the case of Hamiltonian flows or $2M$–dimensional symplectic maps with $2M > 2$, the SALI fluctuates around a non-zero value for regular orbits, while it tends exponentially to zero for chaotic orbits [1, 4, 5], following a rate which depends on the difference of the two largest Lyapunov Exponents [6]. Thus, in 2D and 3D Hamiltonian systems the distinction between ordered and chaotic motion is easily done. On the other hand, in the case of 2D maps the SALI tends to zero both for regular and for chaotic orbits, following however completely different time rates, which again allows us to distinguish between the two cases [1].

3. Global dynamics of 2D Standard map

As a simple 2D map which exhibits regular and chaotic behavior, we consider the well–known standard map [19] having the form

$$\begin{aligned} x_{n+1} &= x_n + y_{n+1} \\ y_{n+1} &= y_n + \tfrac{K}{2\pi}\sin(2\pi x_n) \end{aligned} \quad (mod\ 1)\ , \tag{6}$$

where K is the so–called non–linear parameter of the system.

Before studying the global dynamics of map (6) let us look in more detail the behavior of SALI for regular and chaotic orbits of a 2D map. In the case of a chaotic orbit any two deviation vectors will be aligned to the direction defined by the largest Lyapunov exponent L_1, and consequently SALI tends to zero following an exponential decay of the form SALI $\propto e^{-2L_1 n}$, with n being the number of iterations [6]. In the case of regular orbits any two deviation vectors tend to fall on the tangent space of the torus on which the motion lies [1, 4, 7]. For a 2D map this torus is an 1–dimensional invariant curve, whose tangent space is also 1–dimensional and consequently any two deviation vectors will become aligned. Thus, even in the case of regular in 2D maps SALI tends to zero. This decay follows a power law [1] having the form SALI $\propto 1/n^2$ [7].

In figure 1 we see the different behavior of SALI for regular and chaotic orbits of the standard map (6). It is exactly this different behavior of the index that allows us to use SALI for a fast a clear distinction between regions of chaos and order in the 2–dimensional phase space of the standard map. From the results of figure 1 and the theoretical predictions for the evolution of SALI we see that after $n = 500$ iterations the value of SALI of a regular orbit becomes of the order of 10^{-6}, while for a chaotic orbit SALI has already reached extremely small values. Thus, the percentage of chaotic orbits for a given value of K can be computed as follows: We follow the evolution of orbits whose initial conditions lie on a 2–dimensional grid of 1000×1000 equally spaced points on the (x_n, y_n) plane and register for each orbit the value of SALI after $n = 500$ iterations. All orbits having values of SALI significantly smaller than

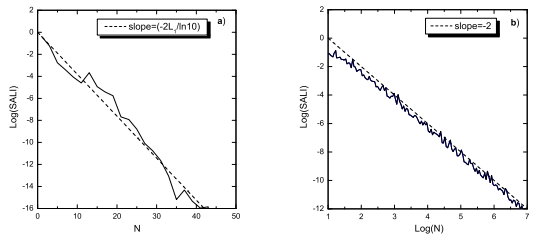

FIG. 1. The evolution of SALI (solid lines) for a) the chaotic orbit with initial condition $x_0 = 0.2$, $y_0 = 0.2$ and b) the regular orbit with initial condition $x_0 = 0.4$, $y_0 = 0.8$ of the standard map (6) for $K = 2$, with respect to the number of iterations n. Note the different scales of the horizontal axis. The Lyapunov exponent of the chaotic orbit is $L_1 \approx 0.438$. Dashed curves in panels a) and b) correspond to functions proportional to $e^{-2L_1 n}$ and $1/n^2$ respectively. It is evident that the theoretical predictions for the evolution of SALI describe very well the numerical data.

10^{-6} (which correspond to the value SALI reaches after 500 iterations in the case of regular orbits), are characterized as chaotic. In practice as a good threshold for this distinction we consider the value 10^{-8}. Thus, all orbits having SALI $\leq 10^{-8}$ after $n = 500$ iterations are characterized as chaotic, while all other orbits are considered as non–chaotic.

In figure 2a) we present the outcome of this procedure for $K = 2$. Each initial condition is colored according to the color scale seen at the right side of the panel. So, chaotic orbits, having SALI $\leq 10^{-8}$ are colored black, while light gray color corresponds to regular orbits having high values of SALI. Thus, in figure 2a) we can clearly identify even tiny regions of regular motion which are not easily seen in phase space portraits of the map (figure 2b)). Using the above–

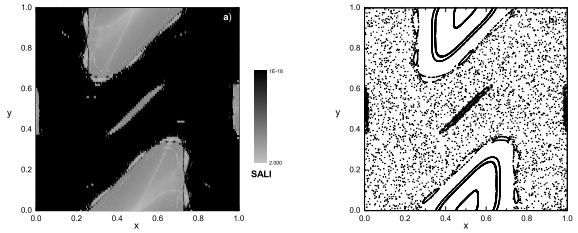

FIG. 2. a) Regions of different values of SALI after $n = 500$ iterations of map (6) for $K = 2$. b) Phase space portrait of map (6) for the same value of K.

described method we were able to compute very fast and accurately the percentages of regular motion for large values of parameter K. In figure 3a) we plot the percentage of regular orbits for $180 \leq K \leq 200$ where K varies with a step $\delta K = 0.001$. A blow-up of the pick appearing close to $K = 188$ is seen in figure 3b). In order to accelerate the numerical computation we applied the following technique: For each orbit we compute its SALI value at $n = 500$, keeping also track of squares on the (x, y) plane that the orbit visits in its evolution. Then, we attribute this SALI value to all these squares. In this way we gain considerably in computational time, since it is not necessary to perform the same computation for the total number of the initial conditions. For each value of K a grid of 1000×1000 initial conditions were used, allowing us to detect extremely tiny regions of regular motion (note that the percentages of regular orbits in figure 3 remain always less than 0.0015%!). From the results of figure 3 we see a periodicity of period 2π in the appearance of island of stability as K varies, in accordance to the results presented in [20]. In our study we were able to reproduce the results obtained in [20] but with considerably less computational effort. For example, for $K = 2$ instead of using all the 10^6 initial conditions of the 1000×1000 grid, computing the evolution of only 12425 initial conditions up to $n = 500$ iterations was sufficient for characterazing the total 10^6 points. Thus, for $K = 2$ we were able to compute the percentage of regular orbits on a 1000×1000 grid mesh by computation only $3 \times 500 \times 12425 \approx 2 \cdot 10^7$ iterations of the map (6) and its tangent map, instead for the $5 \cdot 10^9$ iterations needed for obtaining the same result in [20]. In particular for the computation of the data of figure 3 we needed only 27 hours of CPU time on an Athlon 64bit, 3.2Ghz PC.

4. Applications to 2D and 3D models of barred galaxies

4.1. The model

A 3D rotating model of a barred galaxy can be described by the Hamiltonian function:

$$H = \frac{1}{2}(p_x^2 + p_y^2 + p_z^2) + V(x, y, z) - \Omega_b(xp_y - yp_x). \quad (7)$$

The bar rotates around its z-axis, while the x-axis is along the major axis and the y-axis is along the intermediate axis. The p_x, p_y and p_z are the canonically conjugate momenta. Finally, V is the potential, Ω_b represents the pattern speed of the bar and H is the total energy of the system.

The potential V of our model consists of three components:

1. A *disc*, represented by a Miyamoto disc [21]:

$$V_D = -\frac{GM_D}{\sqrt{x^2+y^2+(A+\sqrt{z^2+B^2})^2}}, \qquad (8)$$

where M_D is the total mass of the disc, A and B are the horizontal and vertical scalelengths, and G is the gravitational constant.

2. A *bulge* which is modeled by a Plummer sphere with the potential:

$$V_S = -\frac{GM_S}{\sqrt{x^2+y^2+z^2+\epsilon_s^2}}, \qquad (9)$$

where ϵ_s is the scalelength of the bulge and M_S is its total mass.

3. A triaxial Ferrers *bar*, the density $\rho(x)$ of which is:

$$\rho(x) = \begin{cases} \rho_c(1-m^2)^2 & , m<1 \\ 0 & , m \geq 1 \end{cases}, \qquad (10)$$

where $\rho_c = \frac{105}{32\pi}\frac{GM_B}{abc}$ the central density, M_B is the total mass of the bar and

$$m^2 = \frac{x^2}{a^2}+\frac{y^2}{b^2}+\frac{z^2}{c^2}, \qquad a>b>c>0, \qquad (11)$$

with a, b and c are the semi-axes and M_B the mass of the bar component. The corresponding potential is:

$$V_B = -\pi Gabc\frac{\rho_c}{n+1}\int_\lambda^\infty \frac{du}{\Delta(u)}(1-m^2(u))^{n+1}, \qquad (12)$$

where

$$m^2(u) = \frac{x^2}{a^2+u}+\frac{y^2}{b^2+u}+\frac{z^2}{c^2+u} \qquad (13)$$

and

$$\Delta^2(u) = (a^2+u)(b^2+u)(c^2+u) \qquad (14)$$

The corresponding forces are given analytically in [22].

This model has been used extensively for orbital studies [23–27].

4.2. Numerical results

We first applied the SALI method to the 2D bar potential resulting from the restriction of our study on the $z = p_z = 0$ subspace of the whole phase space of the system. It can be easily seen that, due to the symmetries of Hamiltonian (7), orbits starting with $z = p_z = 0$ remain for all time on the (x, y) plane. In this case, the Hamiltonian function governing the motion is derived by setting $z = p_z = 0$ to equations (7)–(14) and the corresponding Poincaré Surface of Section (PSS) is 2–dimensional and can be easily visualized.

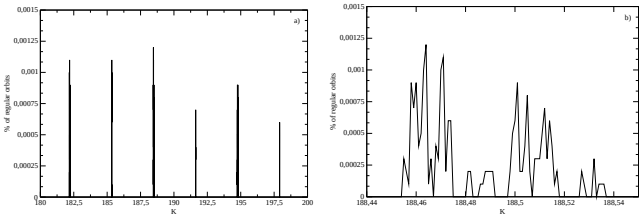

FIG. 3. a) Percentages of regular orbits of map (6) as a function of the nonlinear parameter $K \in [180, 200]$, b) A zoom of panel a) in the region of $K \in (188.44, 188.55)$.

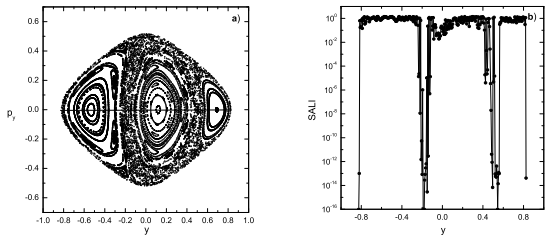

FIG. 4. a) Poincaré surface of section for the $2D$ Ferrers' model in (y, p_y) - plane for $H = -0.360$, b) The variation of the SALI value for initial conditions chosen on the line $y = 0$ of the corresponding PSS of panel a).

As we have already mentioned, in 2D Hamiltonian systems SALI tends exponentially to zero for chaotic orbits, while it fluctuates around a positive number for regular orbits. In figure 4a) we present the PSS (plane (y, p_y)) of the system for $H = -0.360$, which exhibits both regular and chaotic regions. By choosing initial conditions on the line $p_y = 0$ of the PSS and calculating their SALI values we were able to detect very small regions of stability that can not be visualized easily on the PSS. We plot the corresponding values of the SALI in figure 4b). The values of the SALI tend to zero ($\approx 10^{-16}$), for the initial conditions chosen inside the chaotic regions of the PSS, contrary to the initials conditions inside the stability islands whose SALI values retain large positive values. Repeating this procedure for initial conditions on the whole (y, p_y) plane, for several values of the energy, we were able to follow the change of the fraction of chaotic and regular orbits in the phase space as the value of H varies.

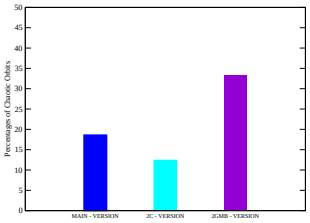

FIG. 5. Comparison of the percentages of chaotic orbits for the main model, a model with twice the length of the short axis (2C - version) and a model with twice the bar mass (2GMB - version). The initial conditions in the plane (x, p_y, z) with $(y, p_x, p_z) = (0, 0, 0)$

We have also studied the full 3D model, as well as other models with different bar mass and different values of the semi-minor axis c. In each case we considered two sets of initial conditions. The first set includes orbits with initial conditions in the plane (x, p_y, z) with $(y, p_x, p_z) = (0, 0, 0)$ and the second one, orbits with initial conditions in the plane (x, p_y, p_z) with $(y, z, p_x) = (0, 0, 0)$. By comparing the results, we found that the increase of the bar mass causes more chaotic behavior for both sets of initial conditions. In figure 5 we present the change of percentages of the chaotic orbits as the parameters vary for the first set of initial conditions (similar results where found for the second one as well). These findings are in accordance to the results obtained in [28] for the 2D case. On the other hand, it was obvious that when the bar is thicker, i.e. the length of the z-axis larger, the system becomes less chaotic [12]. Finally, we calculated the percentages of chaotic and regular orbits for different values of the pattern speed Ω_b. From the orientation of periodic orbits, Contopoulos [29] showed that bars have to end before corotation, i.e. that $r_L > a$, where r_L the Lagrangian, or corotation, radius. Comparing the shape of the observed dust lanes along the leading edges of bars to that of the shock loci in hydrodynamic simulations of gas flow in barred galaxy potentials, Athanassoula [30, 31] was able to set both a lower and an upper limit to corotation radius, namely $r_L = (1.2 \pm 0.2)a$. This restricts the range of possible values of the pattern speed between a high value that corresponds to the Lagrangian radius $r_L = 1.4a$ and a low value that corresponds to $r_L = 1.0a$. Using the extremes of this range, we investigated how the pattern speed of the bar affects the dynamics the system and found that the percentage of regular orbits is greater in slow bars [17].

5. Conclusions

In this paper, we applied the SALI method to symplectic 2 dimensional maps and to Ferrers barred galaxy models of 2 and 3 degrees of freedom. We presented and discussed our results comparing the SALI index with traditional methods, such as the PSS method for the 2 degrees of freedom, and showed its effectiveness. We used this index for the derivation of more detailed and refined information choosing initial conditions on a plane of a PSS of the 2D map, especially for small stability islands inside big chaotic seas. This permits an easier and more accurate verification of the appearance of islands as the nonlinearity parameter varies. We also calculated percentages of chaotic and regular orbits and the way they change with the main model parameters, for the 3 degrees of freedom case. In more detail, we calculated percentages of chaotic and ordered trajectories, as some important parameters (as the mass, the length of the short z-axis and the pattern speed of the bar) vary in the initial basic model.

Acknowledgments

We thank the European Social Fund (ESF), Operational Program for Educational and Vocational Training II (EPEAEK II), and particularly the Program PYTHAGORAS II, for funding the above work. Visits between the team members were partially funded by the region PACA. T. Manos was partially supported by the "Karatheodory"graduate student fellowship No B395 of the University of Patras and the Marie Curie fellowship No HPMT-CT-2001-00338. Ch. Skokos was supported by the Marie Curie Intra–European Fellowship No MEIF–CT–2006–025678. The first author (T. M.) would also like to express his gratitude to the Institut de Mécanique Céleste et de Calcul des Ephémérides (IMCCE) of the Observatoire de Paris for its excellent hospitality during his visit in June 2006, when part of this work was completed.

References

[1] Ch. Skokos, *J. Phys. A: Math. Gen.*, **34**, 10029, (2001).

[2] Ch. Skokos, Ch. Antonopoulos, T. Bountis and M.

Vrahatis, in *Proceedings of the 4th GRACM*, ed. D. T. Tsahalis, **IV**, 1496. (2002).
[3] N. Voglis , C. Kalapotharakos and I. Stavropoulos, *Mon. Not. R. Astron. Soc.*, **337**, 619, (2002).
[4] Ch. Skokos, Ch. Antonopoulos, T. Bountis and M. Vrahatis, *Prog. Theor. Phys. Suppl.*, **150**, 439, (2003).
[5] Ch. Skokos, Ch. Antonopoulos, T. Bountis and M. Vrahatis, in *Proceedings of the Conference Libration Point Orbits and Applications*, eds. G. Gomez, M. W. Lo and J. J. Masdemont, World Scientific, 653, (2003).
[6] Ch. Skokos, Ch. Antonopoulos, T. Bountis and M. Vrahatis, *J. Phys. A*, **37**, 6269, (2004).
[7] Ch. Skokos, T. Bountis and Ch. Antonopoulos, *submitted*, (2006).
[8] P. Panagopoulos, T. Bountis and Ch. Skokos, *J. Vib. and Acoust.*, **126**, 520, (2004).
[9] A. Széll, B. Érdi, Zs. Sándor and B. Steves, *Mon. Not. R. Astron. Soc.*, **347**, 380, (2004).
[10] C. Kalapotharakos , N. Voglis and G. Contopoulos, *Mon. Not. R. Astron. Soc.*, **428**, 905, (2004).
[11] Ch. Antonopoulos, T. Manos and Ch. Skokos, in *Proceedings of the 1st IC-SCCE*, ed. D. T. Tsahalis, Patras Univ. Press, **III**, 1082, (2005).
[12] T. Manos and E. Athanassoula, *SF2A-2005: Semaine de l'Astrophysique Francaise*, eds. F. Casoli, T. Contini, J. M. Hameury and L. Pagani, EDP-Sciences, Conference Series, 631, (2005).
[13] T. Manos and E. Athanassoula, *5th International Conference: The Fabulous destiny of galaxies: Bridging past and present"*, astro-ph/0510823, (2005).
[14] Ch. Antonopoulos and T. Bountis, *Phys. Rev. E*, **73**, 056206, (2006).
[15] T. Bountis and Ch. Skokos, *Nucl. Instr. Meth. Phys. Res. – Sect. A*, 561, 173, (2006).
[16] Ch. Antonopoulos, T. Bountis and Ch. Skokos, *Int. J. Bif. Chaos*, **16(6)**, 1777, (2006).
[17] T. Manos and E. Athanassoula, *AIP Conference Proceedings, Recent Advances in Astronomy and Astrophysics: 7th International Conference of the Hellenic Astronomical Society*, ed. N. Solomos, **848**, 662, (2006).
[18] R. Capuzzo–Dolcetta, L. Leccese, D. Merritt and A. Vicari, *astro–ph/0611205*, (2006).
[19] B. V. Chirikov, *Phys. Rep.*, **52**, 265, (1979).
[20] R. Dvorak, B. Funk, F. Freistetter, G. Contopoulos, *Proceedings of the 3rd Austrian-Hungarian Workshop on Trojans and related Topics*, eds. F. Freistetter, R. Dvorak and B. Érdi, 185, (2003).
[21] M. Miyamoto and R. Nagai, *PASJ*, **27**, 533, (1975).
[22] D. Pfenniger, *Astr. Astroph.*, **134**, 373, (1984).
[23] Ch. Skokos, P. A. Patsis and E. Athanassoula, *Mon. Not. R. Astron. Soc.*, **333**, 847, (2002).
[24] Ch. Skokos, P. A. Patsis and E. Athanassoula, *Mon. Not. R. Astron. Soc.*, **333**, 861, (2002).
[25] P. A. Patsis, Ch. Skokos and E. Athanassoula, *Mon. Not. R. Astron. Soc.*, **337**, 578, (2002).
[26] P. A. Patsis, Ch. Skokos and E. Athanassoula, *Mon. Not. R. Astron. Soc.*, **342**, 69, (2003).
[27] P. A. Patsis, Ch. Skokos and E. Athanassoula, *Mon. Not. R. Astron. Soc.*, **346**, 1031, (2003).
[28] E. Athanassoula, O. Bienayme, L. Martinet and D. Pfenniger, *Astr. Astroph.*, **127**, 349, (1983).
[29] G. Contopoulos, *Astr. Astroph.*, **81**, 198, (1980).
[30] E. Athanassoula, *Mon. Not. R. Astron. Soc.*, **259**, 328, (1992).
[31] E. Athanassoula, *Mon. Not. R. Astron. Soc.*, **259**, 354, (1992).